Cement and Concrete Composites 123 (2021) 104209

Contents lists available at ScienceDirect

Cement and Concrete Composites

journal homepage: www.elsevier.com/locate/cemconcomp

Self-healing of PE-fiber reinforced lightweight high-strength engineered cementitious composite

Kequan Yu, He Zhu [1], Mengjun Hou, Victor C. Li [*]

Department of Civil and Environmental Engineering, University of Michigan, Ann Arbor, MI, United States

ARTICLE INFO

Keywords:
Lightweight high-strength engineered cementitious composite
Crumb rubber
Cenosphere
Self-healing
Polyethylene fiber

ABSTRACT

High-strength engineered cementitious composite (HS-ECC) reinforced with polyethylene (PE) fiber typically features larger crack width compared with conventional polyvinyl alcohol fiber-reinforced engineered cementitious composite (PVA-ECC), diminishing the self-healing potential of HS-ECC. This larger crack width is attributed to the high matrix fracture toughness and the weak interfacial property between PE fiber and matrix. In this study, synergistic utilization of crumb rubber (CR) and hollow fly ash cenosphere (FAC) particles as lightweight particles and artificial flaws were employed to reduce the density, the matrix toughness, and the crack width of HS-ECC, leading to a lightweight HS-ECC (LWHS-ECC) with enhanced self-healing capability. The impacts of CR and FAC particles on the density, mechanical, and self-healing properties of LWHS-ECC were investigated. The addition of these two particle types significantly narrows the crack width from 120 μm to 50 μm and promotes the self-healing property of LWHS-ECC. Despite lower compressive and tensile strengths with an increasing amount of CR and FAC, the tensile strength to self-weight ratio of LWHS-ECC is twice that of M45 PVA-ECC. The realization of the self-healing ability of PE-fiber reinforced LWHS-ECC is expected to enlarge its practical application.

1. Introduction

Engineered cementitious composites (ECC) is a special type of fiber-reinforced concrete with distributed microcracks and tensile strain capacity above 3% [1]. The polyvinyl alcohol (PVA) fiber reinforced ECC (PVA-ECC) exhibits a self-controlled crack width around 60 μm, enabling the self-healing capability under various environments [2–6]. The PVA-ECC with narrow crack width enhances the resilience and durability of infrastructures. However, the modest tensile strength of 3–6 MPa [1,7] and the strength-to-density ratio of PVA-ECC may limit its wider application in structural rehabilitation and retrofit.

High-strength engineered cementitious composite (HS-ECC), reinforced by ultra-high molecular weight polyethylene fiber (UHMW-PE, PE for short) has been recently developed [8–12]. HS-ECC features high mechanical strengths and high tensile ductility. The compressive strength of HS-ECC ranges from 80 MPa to over 200 MPa, the tensile strength ranges from 8 to 20 MPa, while the tensile strain capacity of HS-ECC could attain up to 8% depending on the fiber types and fiber parameters (fiber volume, fiber length and diameter) [8–12]. HS-ECC is a promising material for retrofitting unreinforced masonry and corroded reinforced concrete structures [13,14]. However, the crack width of HS-ECC under loads could reach 120–200 μm due to the hydrophobicity of PE fiber and high matrix fracture toughness [15], which is considerably larger than that of PVA-ECC and limits the self-healing potential of HS-ECC [6,7]. The larger crack width and poor autogenous healing property of HS-ECC put this composite at a disadvantage when compared with PVA-ECC. Further, the higher density of HS-ECC could increase the dead load of the repaired or new structures, leading to a larger response under seismic action. Therefore, a HS-ECC that integrates the merits of high tensile strength, lightweightness and self-healing properties would be attractive for the design of efficient structural elements with long service life.

Attempts have been made to decrease the density of HS-ECC by using low-density ingredients including fly ash cenosphere, entrained air, vermiculite, and crumb rubber [16,17], leading to the density of HS-ECC lower than the threshold value for lightweight concrete of 1850 kg/m^3 [18]. The compressive and tensile strength ranges of these lightweight HS-ECC are 40–70 MPa and 7–9 MPa, respectively [16,17]. The specific

* Corresponding author.
E-mail address: vcli@umich.edu (V.C. Li).
[1] Co-first author.

https://doi.org/10.1016/j.cemconcomp.2021.104209
Received 12 January 2021; Received in revised form 24 June 2021; Accepted 3 August 2021
Available online 8 August 2021

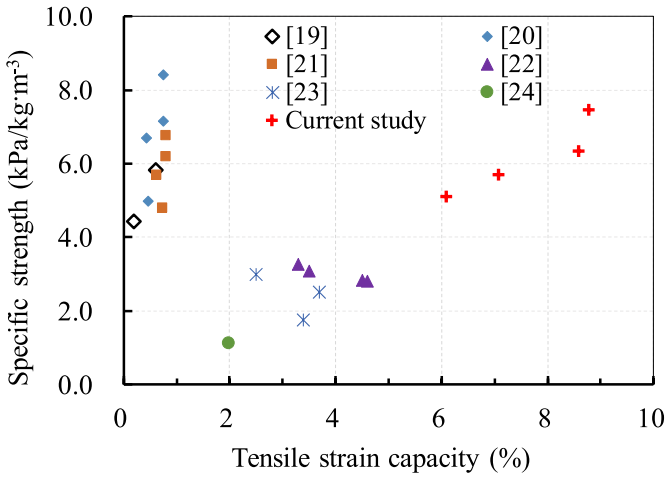

Fig. 1. Specific tensile strength of high-performance concretes.

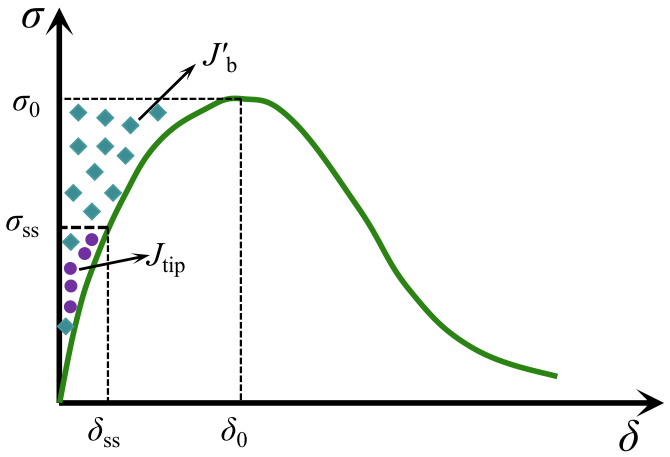

Fig. 2. Typical crack bridging stress vs crack opening (σ-δ) relation. The diamond shaded area is J'_b. J_{tip} at steady-state crack extension is indicated by purple dot-shaped area. (For interpretation of the references to colour in this figure legend, the reader is referred to the Web version of this article.)

tensile strengths (tensile strength-to-density ratio) combined with tensile strain capacity of lightweight high-strength ECC (LWHS-ECC) are remarkably higher than those of ultra-high-performance concrete (UHPC) and PVA-ECC (Fig. 1) [19–24], increasing the repair efficiency for infrastructure. The inherently low thermal conductivity of LWHS-ECC is promising for the integrated structural-plus-energy retrofitting of old masonry and/or cultural heritage buildings, protecting the residents during earthquakes, whilst increasing the energy performance of these buildings. Further, these induced lightweight particles could simultaneously act as the artificial flaws lowering the fracture toughness K_m of the matrix and thereby increasing the multiple cracking robustness and reducing the crack width of HS-ECC [16,17]. Despite these developments, previous LWHS-ECC has not been endowed with the self-healing capability due to the relatively large crack width [16,17]. Therefore, to what an extent the crack width of LWHS-ECC could be reduced and whether LWHS-ECC possesses self-healing capacity are two questions that remain to be answered.

This research aims to develop a self-healing LWHS-ECC by synergistic utilization of crumb rubber (CR) and hollow fly ash cenosphere (FAC) particles as lightweight ingredients and artificial flaws. The physical and mechanical performances of LWHS-ECC with different lightweight particle replacement ratios (i.e., 25%, 40% and 50% of the dry ingredients by mass) were assessed. The specific tensile strength of LWHS-ECC was compared to that of M45 PVA-ECC. Further, the self-healing capacity and properties of pre-cracked (after imposing strains of 0.5%, 1.0%, 2.5% and 4.5%) LWHS-ECC subjected to wet-dry cycles were evaluated. The rate and extent of self-healing behavior were quantified by resonant frequency, permeability and tensile performance.

2. Design theory

Based on the micromechanical model, two criteria (strength criterion and energy criterion) should be satisfied to achieve the strain-hardening performance and multi-cracking states [25,26]. The strength criterion requires the matrix tensile cracking strength σ_c to be less than the maximum fiber bridging strength σ_0.

$$\sigma_c < \sigma_0 \tag{1}$$

where σ_c is governed by the matrix fracture toughness K_m and preexisting internal flaw size a_0; in the present study, σ_c is taken as the first crack strength [27].

The energy criterion requires the crack tip toughness J_{tip} to be less than the complementary energy J'_b, calculated from the fiber-bridging constitutive relationship, i.e., bridging stress σ versus crack opening δ (σ-δ curve), as illustrated in Fig. 2.

$$J_{tip} \le \sigma_0\delta_0 - \int_0^{\delta_0} \sigma(\delta)d\delta \equiv J'_b \tag{2}$$

$$J_{tip} = \frac{K_m^2}{E_m} \tag{3}$$

The strength criterion Eq. (1) governs the initiation of crack and the energy criterion Eq. (2) controls the crack propagation mode. Both criteria are indispensable to achieving the strain-hardening performance of LWHS-ECC. While the satisfaction of Eqs. (1) and (2) ensures the occurrence of multi-cracking, the high tensile ductility of ECC and the number of cracks that can develop (the multi-cracking saturation level) are governed by the flaw size and its distribution [28]. Limited by the peak bridging stress σ_0 at the weakest cross-section, a lower bound of

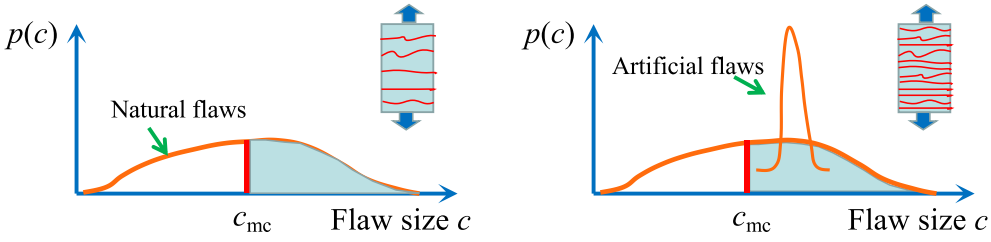

(a) Size distribution of natural flaws (b) Size distribution of natural and artificial flaws

Fig. 3. Size distribution of flaws (adapted from Ref. [31]). The shaded region represents flaws large than c_{mc} that are activated during the strain-hardening stage of tensile loading.

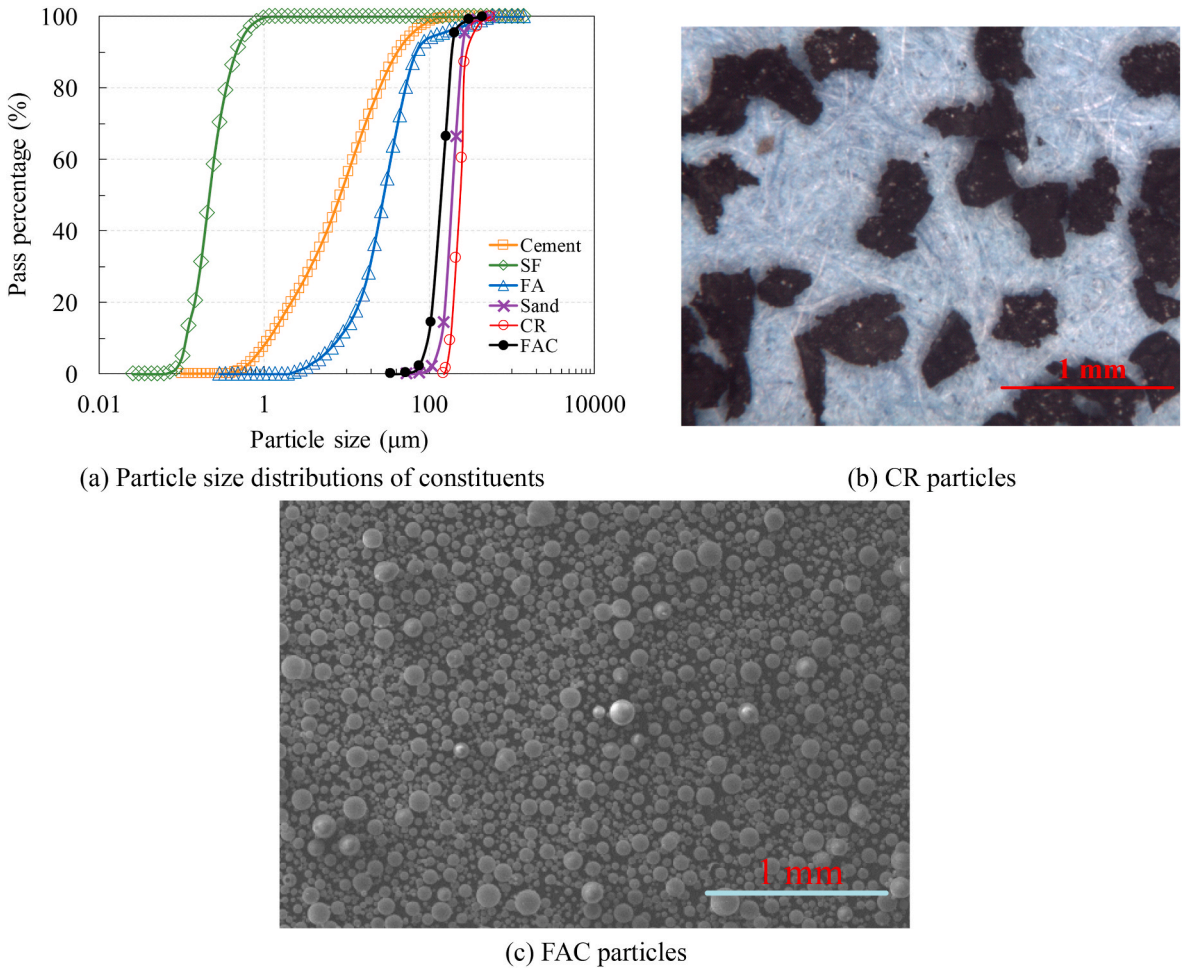

(a) Particle size distributions of constituents

(b) CR particles

(c) FAC particles

Fig. 4. Particle size distributions of constituents, CR and FAC particle morphology.

Table 1
Mix proportion of LWHS-ECC.

ID	Cement kg/m^3	Silica fume kg/m^3	Fly ash kg/m^3	Sand kg/m^3	FAC kg/m^3	CR kg/m^3	Water kg/m^3	SP kg/m^3	Fiber kg/m^3
M-0	650	150	700	550	–	–	240	25	19.4
M-25	650	150	700	–	–	183.3	240	25	19.4
M-40	552.5	127.5	595	–	105	183.3	240	25	19.4
M-50	455.0	105.0	490	–	150	183.3	240	25	19.4

Note: The solid content of SP is 40%.

critical flaw size c_{mc} is set and only those flaws larger than c_{mc} could be activated before the ultimate tensile strength is reached (Figs. 3a and 4). A large margin for these criteria is preferred to achieve robust ductility of ECC, as demonstrated in normal and high-strength PE-ECC [8,12]. However, the crack width of PE-ECC reaches 120–200 μm, which limits its capacity for self-healing [29]. Therefore, a design method to reduce the crack width of PE-ECC is needed.

Deliberate planting of artificial flaws such as polypropylene beads and superabsorbent polymers with the proper size has been shown to be effective in activating more micro-cracks (Fig. 3b) [30,31]. The addition of artificial flaws could remarkably reduce the matrix fracture toughness and cracking strength, while slightly diminishing the fiber-bridging strength, leading to a reduction in the fiber-bridging transition length between adjacent cracks (i.e., crack spacing) and thus a larger number of cracks. The weaker matrix strength also results in a smaller crack width during the tension process [32] and increases the self-healing capacity of PE fiber-reinforced LWHS-ECC.

In the current study, FAC particles are used as lightweight fillers to reduce the density as well as the matrix fracture toughness, shifting the critical flaw size to the left (Fig. 3b) and activating more cracks. However, the crack width of this lightweight ECC is still too large to be self-healed [16,17]. The CR particles act as both the artificial flaws and lightweight ingredients to activate more microcracks and reduce crack width to ensure the self-healing potential of LWHS-ECC.

3. Sample preparation

3.1. Raw constituents and mixture preparation

The mix proportion of LWHS-ECC consists of four parts, i.e., the binder materials, aggregate, lightweight particles and reinforcing PE fiber (Table 1, Shangdong Aidi Co. China). The binder materials include ordinary Portland cement PO 52.5R (Type I, Lafarge Holcim Cement Co.), silica fume (SF, Elken Co.), and fly ash (FA, Boral Material Technologies Inc.). These materials along with the low water-to-binder ratio generate sufficient C–S–H gel and homogenize the matrix to produce a

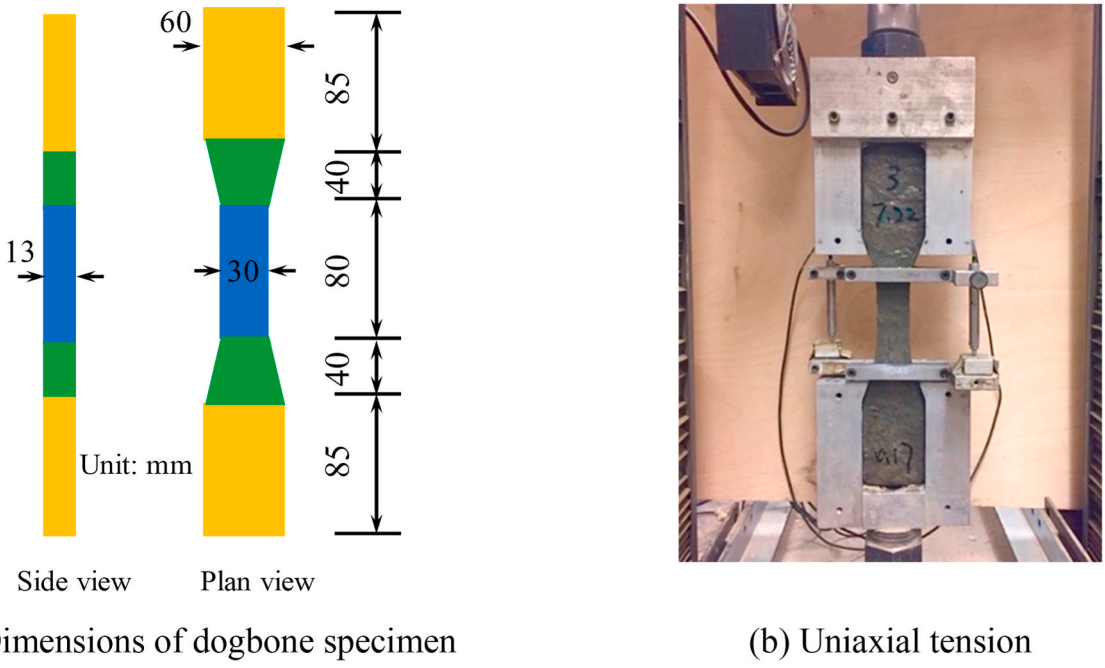

Fig. 5. Specimen dimensions and test setup.

Table 2
Test scheme of LWHS-ECC.

Mix proportions	Number of specimens		
	Compression	Tension	Matrix three-point bending
M − 0, M − 25, M − 40, M-50	5	5	6
M-50-0.5%, 1.0%, 2.25%, 4.5%	N/A	5	N/A

high compressive strength under normal curing conditions (20 ± 1 °C and 40 ± 5% RH). F75 fine silica sand (US Silica Co.) was used as the aggregate in the reference mixture.

Two lightweight particles, i.e., fly ash cenosphere (FAC, Cenostar Co.) and crumb rubber (CR, Entech Co.) were employed to replace the solid ingredients of the HS-ECC to reduce the density and act as the artificial flaws. FAC particle has a mean particle size of 110 μm and was used to partially replace the binder materials in the reference mix (Table 1) to reduce the density of HS-ECC. CR particle with particle size larger than that of silica sand was used to replace the silica sand in the mixes, while excessive CR particle would significantly reduce the viscosity of the HS-ECC matrix and disturb the fiber dispersion. The particle size distributions of binder materials, silica sand and lightweight particles are shown in Fig. 1. Besides the lightweightedness function, CR particles with a larger particle size as well as lower bond strength to matrix act as artificial flaws of LWHS-ECC to activate more cracks under tension.

The replacement ratios of lightweight particles to the solid ingredients (binder materials and aggregate) in the reference mix are 25%, 40% and 50%, respectively. CR and FAC particles have the same density of 900 kg/m^3. The water-to-binder (w/b) ratio of the reference mixture was 0.17 including the water from polycarboxylate-based superplasticizer (SP, MasterGlenium 7920, BASF Co.). SP was used to maintain a proper mix flowability. The mixes were named as M-X, where X represents the replacement ratio of lightweight particles (Table 1).

High-strength polyethylene fiber (PE) was used as the reinforcement of LWHS-ECC specimens. PE fiber has a density of 970 kg/m^3 and a tensile strength of 2400 MPa. Its diameter and length are 24 μm and 18 mm, respectively, resulting in an L_f/d_f ratio of 750 [33,34]. The PE fiber content is 2% by volume for all four mixes.

3.2. Mechanical performance tests

Plain dogbone specimens (Fig. 5a) were employed to determine the uniaxial tensile performance of LWHS-ECC, including the mechanical properties and crack parameters. The mixture with a sufficiently small crack width was selected for the self-healing study following the procedure in Ref. [29]. Five specimens of each mix were prepared and tested at 28 d. The geometry of the dogbone specimen followed by the JSCE specification ensures the occurrence of most cracks in the central gauge region [35]. Fig. 5b shows the uniaxial tensile test setup. A pair of displacement transducers were attached to measure the elongation within the gauge length to obtain the strain capacity of LWHS-ECC. The real-time tensile load was recorded with a loading rate of 0.5 mm/min. The compressive strengths were determined using 50.8 mm (2 inches) cube specimens at 28 d, respectively. The detailed test scheme is shown in Table 2.

The fracture toughness of LWHS-ECC matrix (without fiber) was conducted using three-point bending test according to specification [36]. The specimen dimensions were 40 mm × 40 mm × 180 mm with a span/depth ratio equal to 4.0, and an initial crack length/specimen depth of 0.3.

3.3. Self-healing tests

To evaluate the rate and extent of self-healing performance of LWHS-ECC, the resonant frequency (RF), permeability and tensile performance of specimens before and after healing were measured and analyzed. It is noted that both the RF and permeability parameters are determined in the unloaded state.

Dogbone specimens of M − 50 were pre-loaded to four tensile strain levels, i.e., 0.5%, 1.0%, 2.25% and 4.5% at 28d (Table 2). The pre-cracked specimens were then exposed to wet-dry cycles comprising 48h water immersion (20 ± 1 °C) and 48h air curing (20 ± 1 °C and 40 ± 5% RH). The wet-dry cycle serves as an accelerated test method to simulate outdoor environments. Five specimens were tested in each case (M-50-0.5%, 1.0%, 2.25% and 4.5%). After 7 wet-dry cycles (28d), the

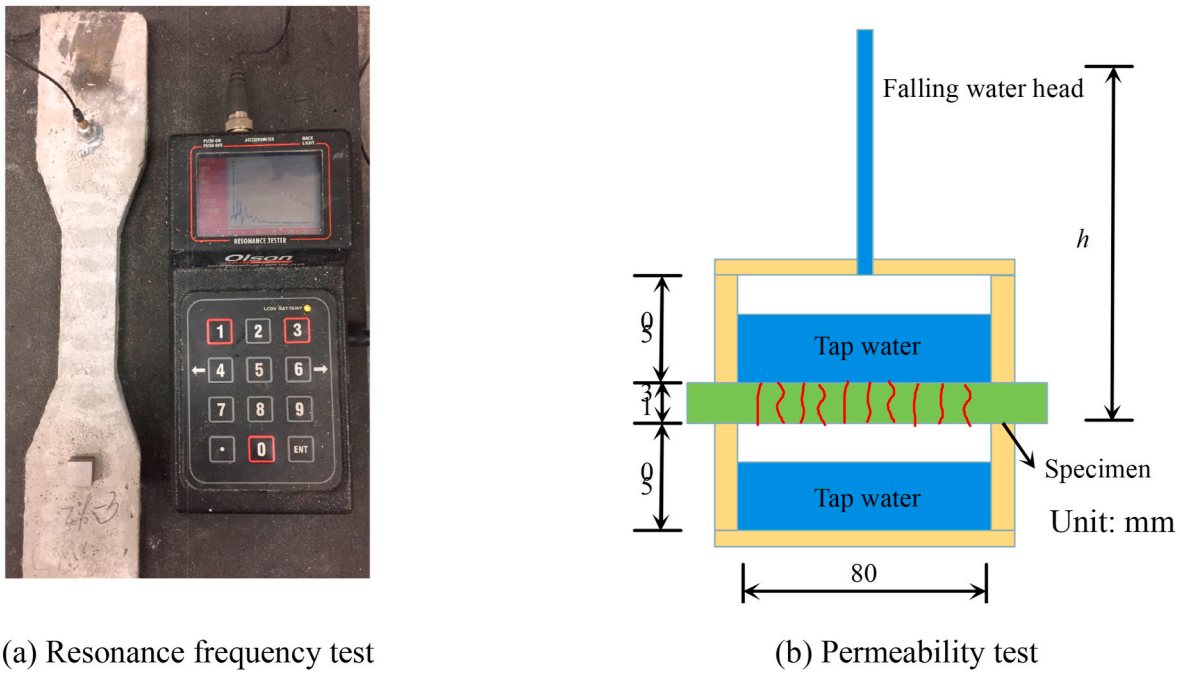

Fig. 6. Self-healing tests.

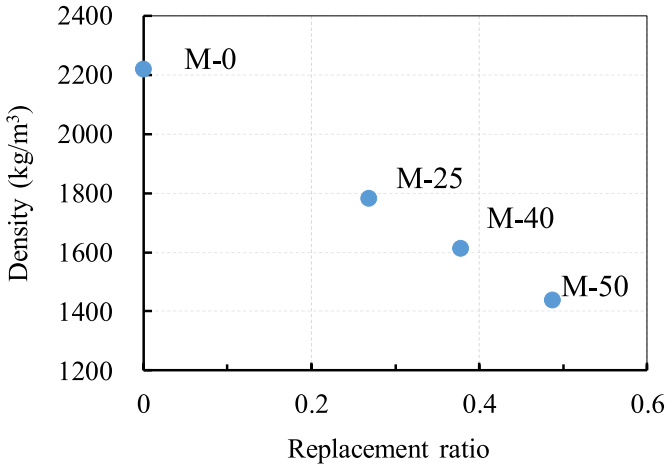

Fig. 7. Density evolution of LWHS-ECC.

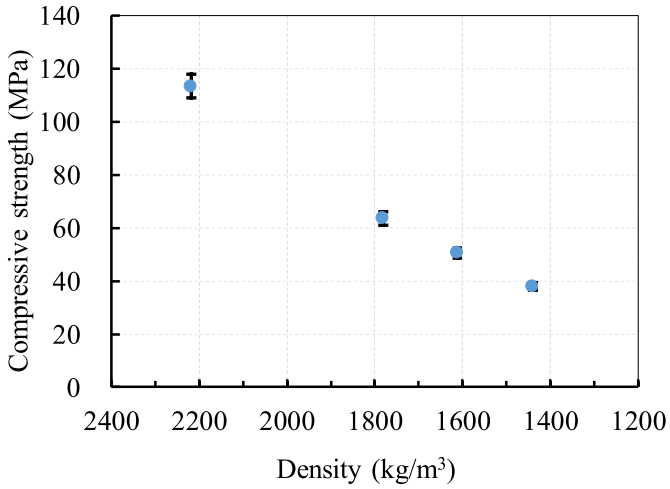

Fig. 8. Compressive strength of LWHS-ECC.

pre-cracked specimens were tested under uniaxial tension until failure [2,5]. The tensile strengths and strain capacity were used to evaluate the self-healing performance of LWHS-ECC.

Longitudinal resonant frequency (RF) measurements (Fig. 6) based on ASTM C215 were carried out to monitor the extent and rate of autogenous healing [37]. Both the intact and pre-damaged specimens were measured after each wet-dry cycle. The normalized RF, i.e., the ratio of the resonant frequency of LWHS-ECC at any given pre-loaded strain divided by that of virgin LWHS-ECC without pre-damage, was measured (Eq. (4)). The change of resonant frequency is used as an indicator to quantify the damage degree of pre-cracked LWHS-ECC specimens and the recovery degree of healed specimens.

$$R_{RF} = \frac{RF_{\varepsilon}}{RF_0} \tag{4}$$

where RF_{ε} is the RF value of preloaded specimens under tensile strain ε exposed to wet-dry cycle. The RF_0 is the RF value of intact specimens exposed to the same wet-dry cycles. A higher R_{RF} value reflects higher

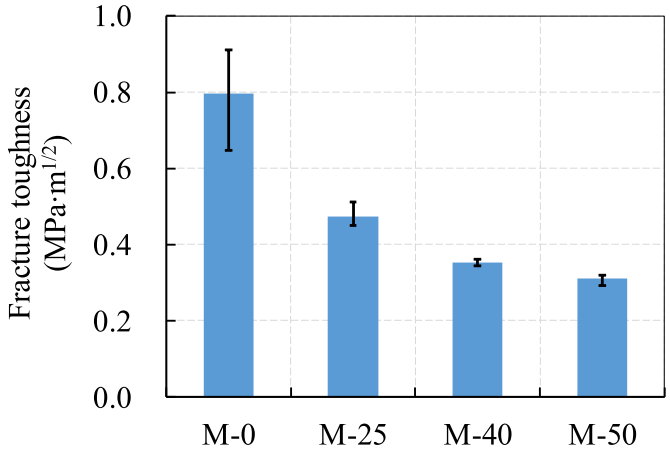

Fig. 9. Fracture toughness of LWHS-ECC matrix.

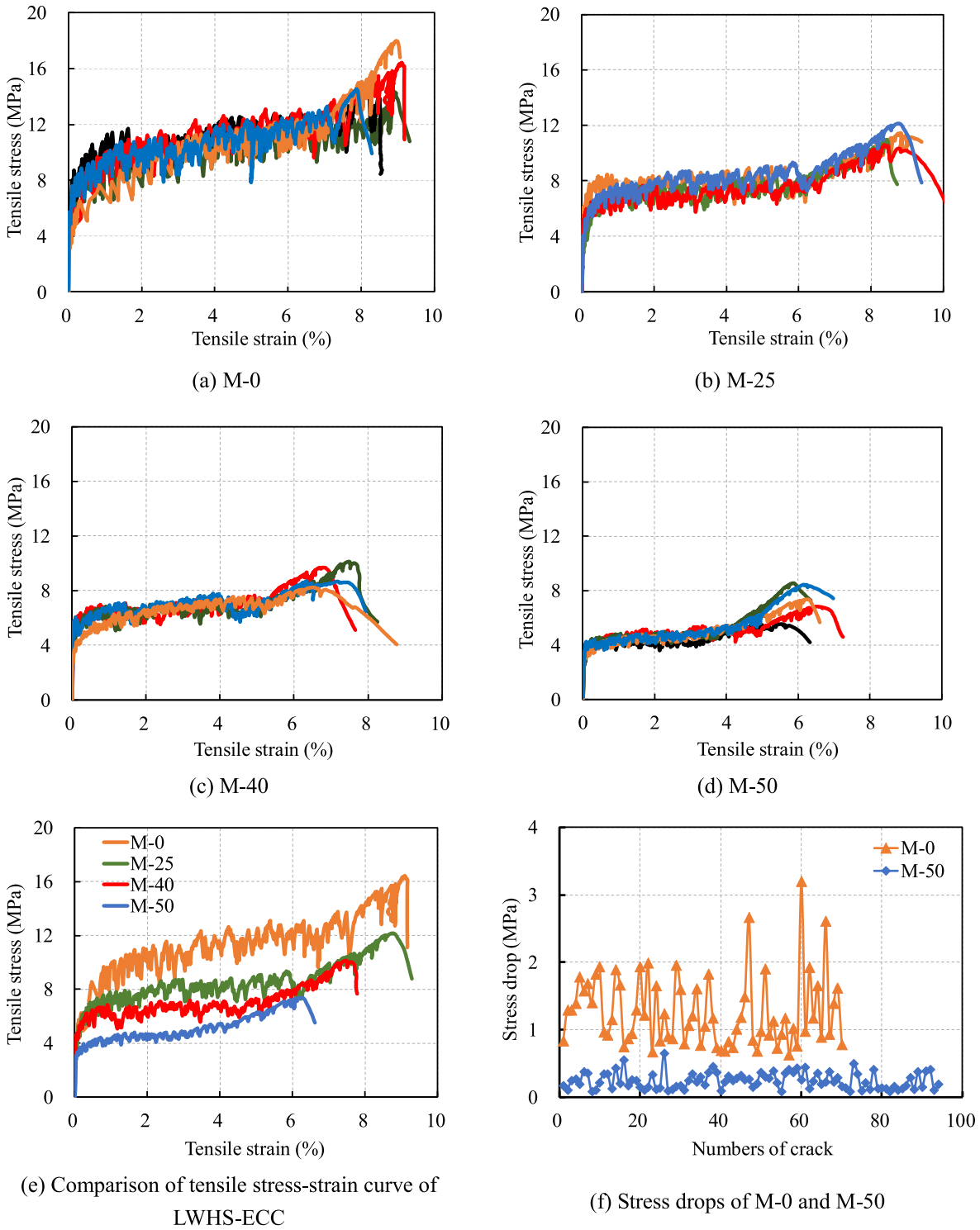

Fig. 10. Tensile stress-strain curves of LWHS-ECC.

recovery ability.

Permeability tests reveal the extent of self-healing. The falling head test (Fig. 6b) was used to determine the permeability of pre-cracked and healed LWHS-ECC specimen at the unloaded state. The permeability test was conducted at a standard room temperature of 20 ± 1 °C. The water head was monitored and recorded starting at 2h after filling the water tank [38]. The permeability coefficient k is determined by the following equation.

$$k = \frac{a}{A}\frac{L}{t_f}\ln\left(\frac{h_0}{h_f}\right) \quad (5)$$

where a is the cross-section area of the standpipe (mm^2), L is the specimen thickness (mm), A is the specimen cross-section area (mm^2), t_f is the test duration (s), h_f and h_0 are the final and initial water head (m).

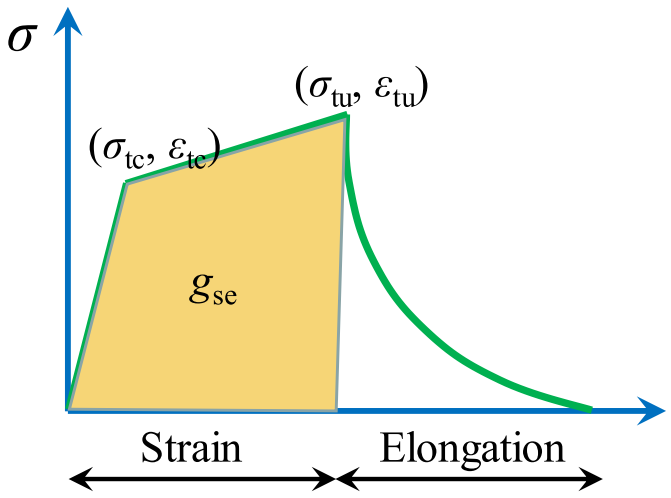

Fig. 11. Schematic tensile parameters.

4. Results and discussion

4.1. Composite density, compressive strength and matrix fracture toughness

Fig. 7 shows the densities of LWHS-ECCs. The density of LWHS-ECC decreases from 2218 kg/m^3 of M − 0 to 1440 kg/m^3 of M − 50 with increasing amount of CR and FAC particles, accompanied by a decrease of compressive strength from 113.4 MPa (M − 0) to 38.0 MPa (M-50; Fig. 8). There is a sharp decrease in the compressive strength from 113.4 MPa of M − 0 to 63.6 MPa of M − 25, a drop of 44%, while the corresponding decrease in density is only 20%. The incompatibility between CR particle and cementitious matrix as well as the lower stiffness and strength of the CR particle significantly damage the interfacial property and internal structure of LWHS-ECC matrix. With a further decrease in density of 20% by using FAC particle (M − 50), the compressive strength drops to 38.0 MPa, narrowly meeting the strength requirement for lightweight high-strength concrete [18].

The fracture toughness of LWHS-ECC matrix decreases with the addition of lightweight particles. Similar to the compressive strength, the fracture toughness of LWHS-ECC decreases sharply from 0.80 MPa•m$^{1/2}$ of M − 0 to 0.47 MPa•m$^{1/2}$ of M-25. The fracture toughness then decreases to 0.31 MPa•m$^{1/2}$ with the replacement ratio of lightweight particles up to 50%. The lower fracture toughness reduces the critical flaw size (Fig. 3), which when combined with the artificial flaw effect of CR particles, leads to more micro-cracks and improves the robustness of the strain-hardening performance of LWHS-ECC. It should be pointed out that robust strain-hardening does not necessarily mean a higher tensile ductility, but more saturated micro-cracks. The lower matrix fracture toughness also decreases the initial cracking stress of LWHS-ECC (Section 4.3).

4.2. Tensile stress-strain curves

Fig. 10 shows the tensile stress-strain curves of LWHS-ECC. All mixes exhibit robust strain-hardening performance. The tensile strain capacities are larger than 6%. Both the ultimate strength and strain capacity of LWHS-ECC decrease with the lightweight particle replacement ratio (Fig. 10e). The strain-hardening process of M − 50 is more stable with

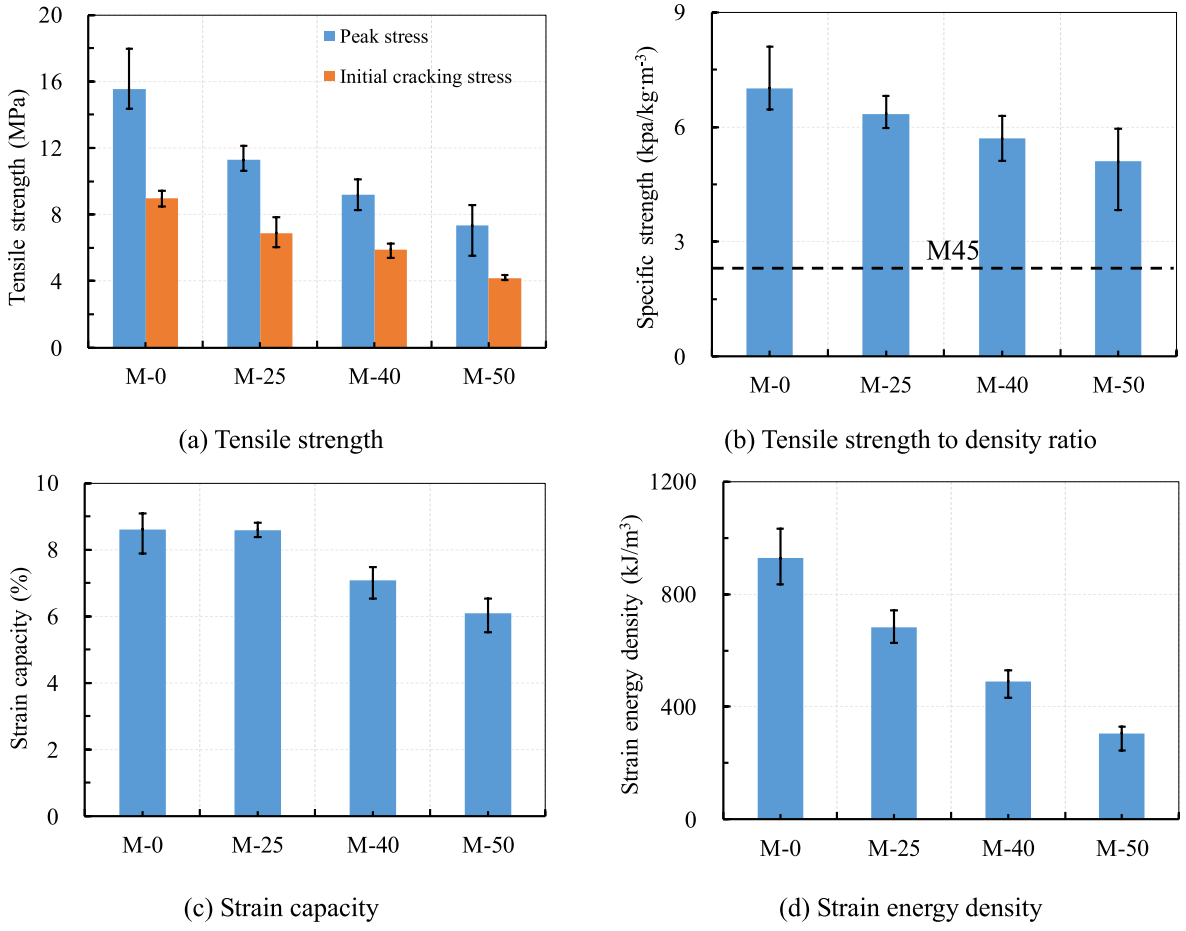

Fig. 12. Tensile parameters of LWHS-ECC.

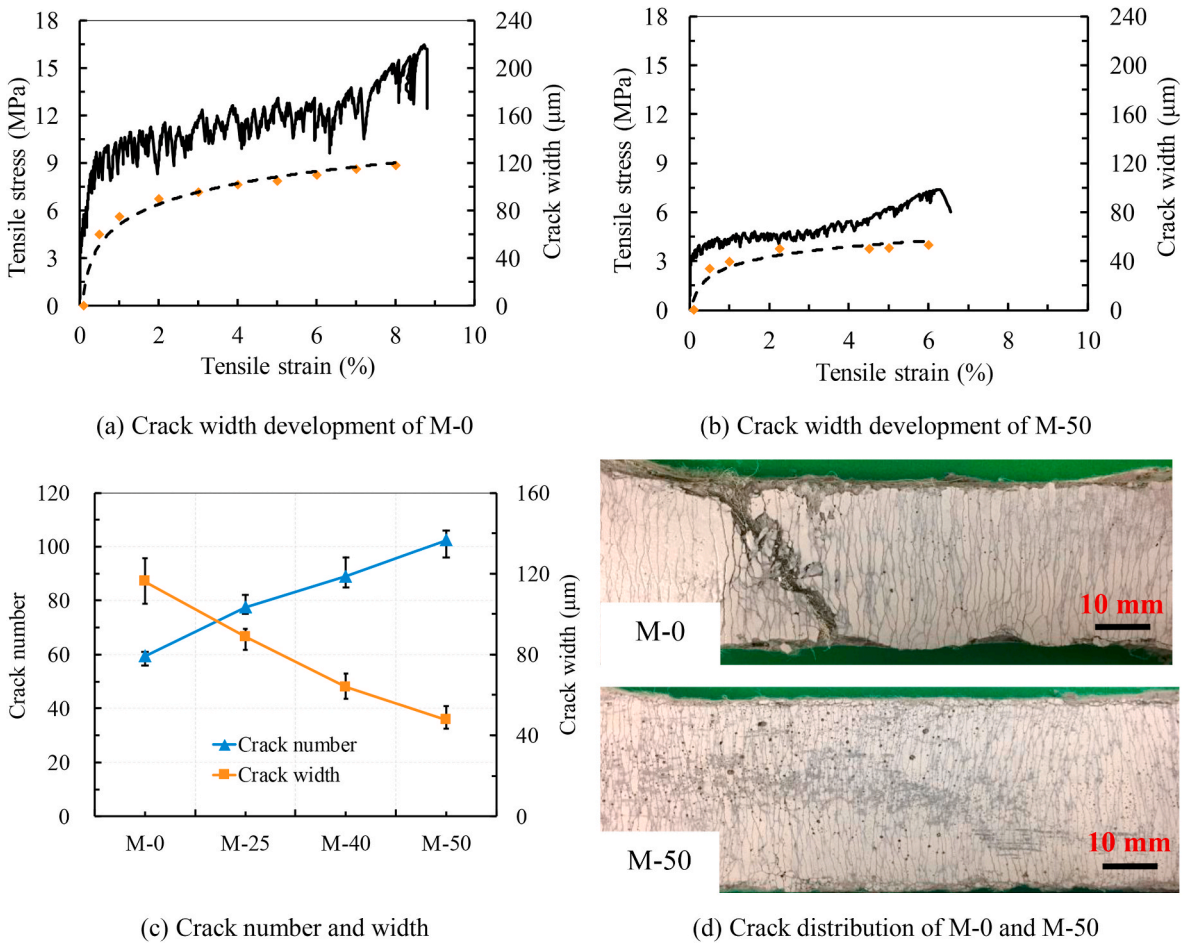

Fig. 13. Crack pattern of LWHS-ECC.

Table 3
Crack parameters of pre-loaded M − 50 at different strain levels.

Tensile strain (%)	Average number of cracks	Average crack width - loaded (μm)	Average crack width - unloaded (μm)
0.5	12	34	18
1.0	21	40	21
2.25	36	50	26
4.5	72	50	27

smaller stress drops during multiple cracking (Fig. 10f). The average stress drops of M − 0 and M − 50 is 1.67 MPa and 0.24 MPa, respectively.

4.3. Tensile mechanical parameters

The tensile parameters of LWHS-ECC, including the peak and initial cracking stress (σ_{tu}, σ_{tc}), the tensile strain capacity (ε_{tu}), and the strain energy density (g_{se}) are shown in Fig. 11 [39].

The tensile parameters of LWHS-ECC are summarized in Fig. 12. The peak stress of LWHS-ECC decreases from 15.55 MPa of M − 0 to 11.29 MPa of M − 25 and 7.34 MPa of M − 50 (Fig. 12a). The addition of CR and FAC particle loosens the matrix structure and lowers the interfacial bond strength between PE fiber and matrix. Further, the larger CR particles disturb the fiber dispersion uniformity, leading to a reduction in the ultimate tensile strength. The initial cracking stress of LWHS-ECC is lowered from 8.98 MPa of M − 0 to 4.18 MPa of M − 50 due to the weakened matrix fracture toughness (Fig. 9) by lightweight particles. It is noticed that the decrease in ultimate tensile strength (52%) is lower

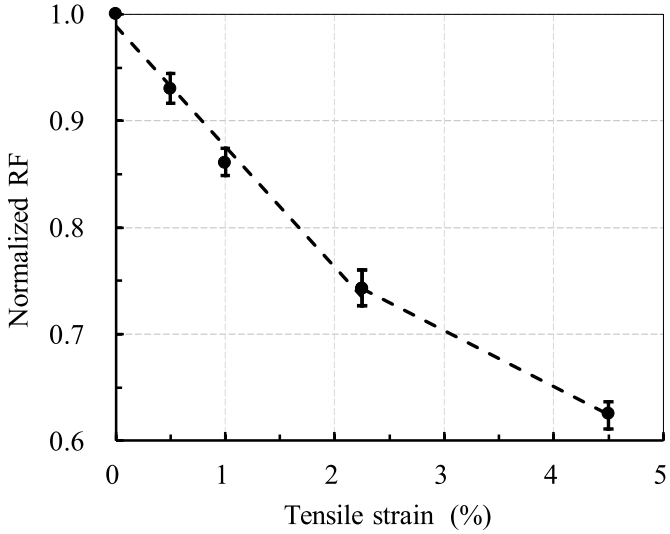

Fig. 14. Normalized RF of pre-cracked M-50.

than that of matrix fracture toughness (62%) due to a gentler decrease in fiber and matrix interfacial bond stress.

The ratio of ultimate tensile strength to compressive strength ranges from 0.14 of M − 0 to 0.20 of M − 50, which is remarkably higher than those of plain concrete, conventional fiber-reinforced concrete and UHPC [19–21]. The reduction in density has a larger impact on

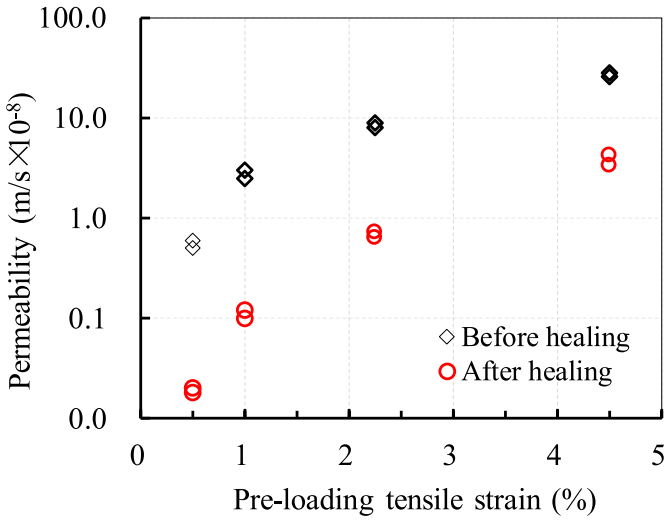

Fig. 15. Permeability of M − 50 before and after healing.

compressive strength than tensile strength. Although the specific strength (ratio of tensile strength to density) of LWHS-ECC decreases with increasing lightweight replacement ratio, the value of M − 50 (4.82) is twice as that of PVA fiber-reinforced M45 (Fig. 12b) [23]. The large specific tensile strength reduces the self-weight of the structural member with the same load capacity.

The strain capacity of LWHS-ECC decreases with the increasing replacement ratio of lightweight particles due to the smaller crack width of these mixtures (M − 25, M − 40, M − 50, Fig. 12c). The strain energy density [39], the area between the strain-hardening branch and the *x*-axis, shares a similar trend with ultimate tensile strength and strain capacity (Fig. 12d). The strain energy density of M − 50 (305.4 kJ/m^3) is 33% of that of M − 0 (928.0 kJ/m^3).

4.4. Crack pattern parameters

Fig. 13a and b shows the crack width development of LWHS-ECC under load (M − 0 and M − 50). The crack width of M − 50 increases significantly up to 2% tensile strain, after which it increases gently and stabilize at around 50 μm, comparable to that of PVA-ECC [23] and endows M − 50 the self-healing potential [29]. The number of cracks increases with the lightweight particle replacement ratio from 60 of M − 0 to 102 of M − 50, while the crack width decreases steadily with the replacement ratio (Fig. 13c). The combination of the artificial flaw and low fracture toughness of the LWHS-ECC matrix activates more micro-cracks and reduces the crack width. The crack distributions on the tensile specimen surfaces of M − 0 and M − 50 are displayed in Fig. 13d.

4.5. Self-healing properties of LWHS-ECC

4.5.1. Pre-damaged M-50

M − 50 specimens with the smallest crack width at ultimate tensile strength were chosen for self-healing studies. The specimens were pre-loaded to four strain levels, i.e., 0.5%, 1.0%, 2.25% and 4.5%. The number of cracks increases with the strain level from 12 at 0.5% to 72 at

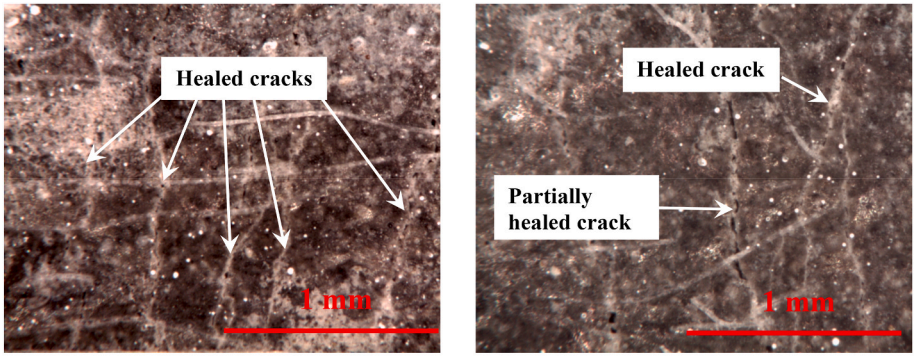

(a) M-50-0.5% (b) M-50-4.5%

Fig. 16. Crack healing in pre-cracked specimens.

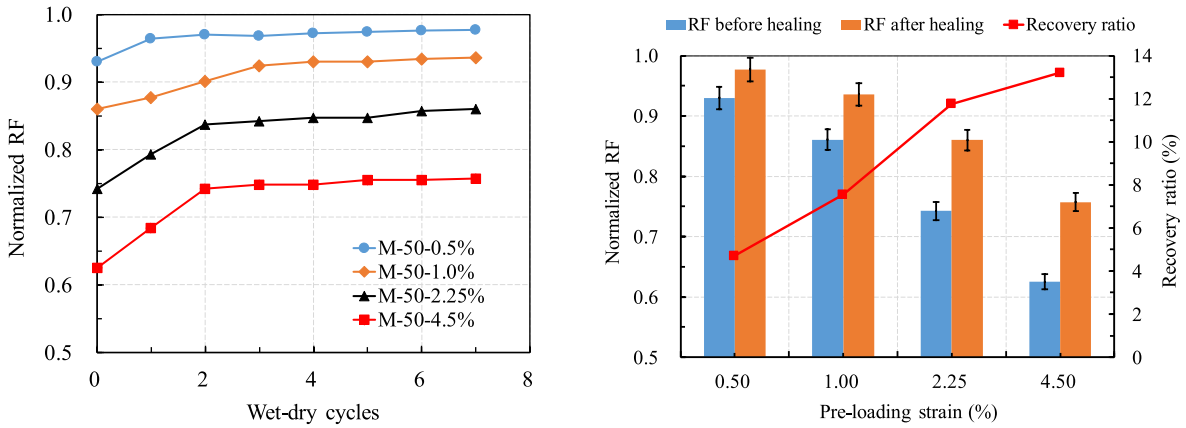

(a) Resonant frequency development (b) Recovery ratio

Fig. 17. Recovery of resonant frequency exposure to wet-dry cycle.

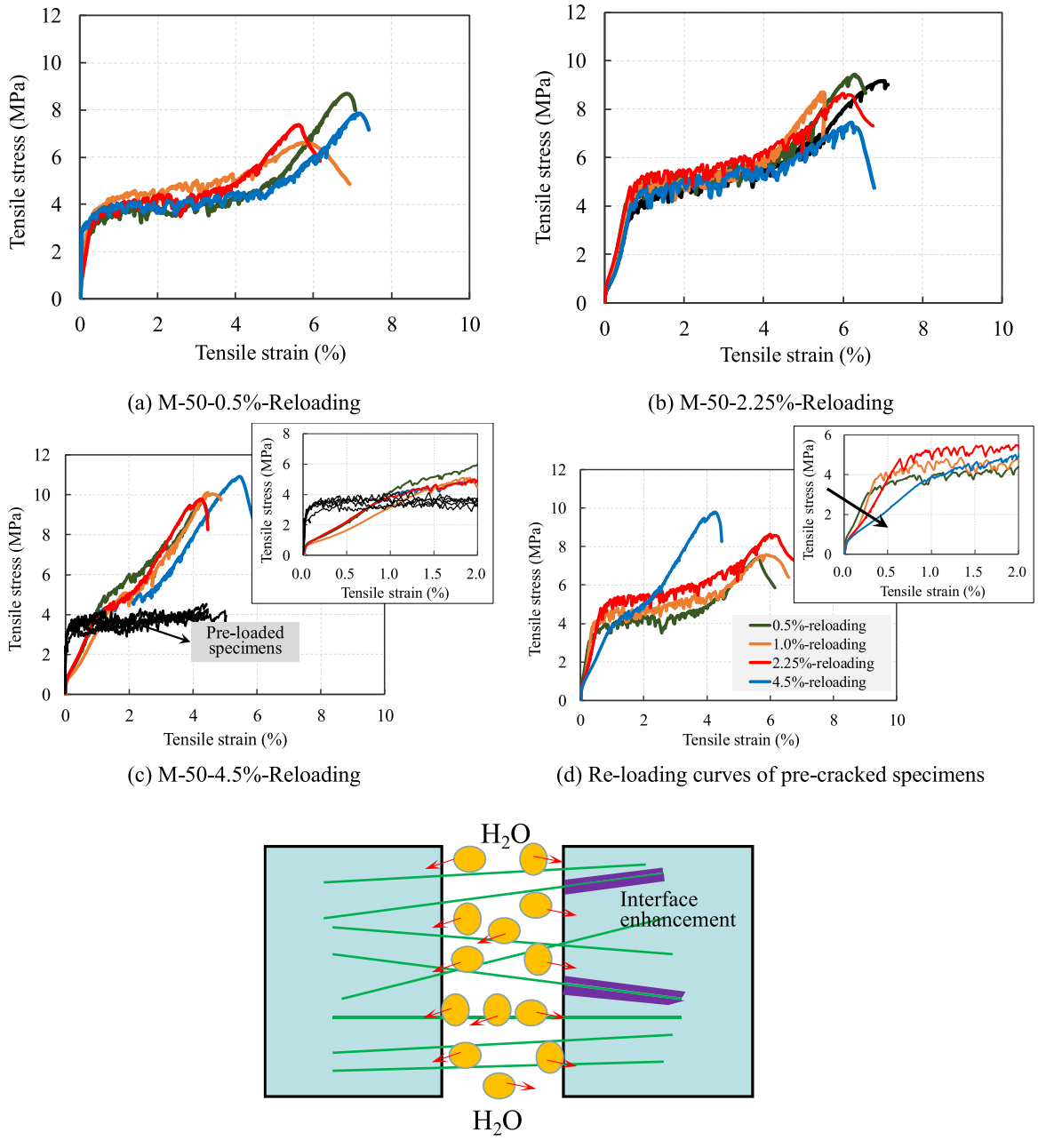

Fig. 18. Reloading tensile stress-strain curves of healed LWHS-ECC specimens.

4.5%, while the average crack width at the loading stage keeps constant at 50 μm after 2.25%. The crack width rebounds by 50% after unloading. The crack numbers and crack widths (at loading and unloading stages) are summarized in Table 3.

The normalized resonant frequency (RF) of pre-cracked LWHS-ECC indicates a bilinear relationship between RF and LWHS-ECC tensile strain deformation (Fig. 14). The bilinear characteristic is attributed to the increase in the number of cracks as well as the crack width at a lower strain level (below 2.25%), while further tensile straining is mainly due to the increase of crack numbers with the average crack width kept constant. This leads to a steeper decrease of RF at smaller strain values followed by a gentler decay at strain values higher than 2.25%. The normalized RF of pre-cracked LWHS-ECC decreases from 0.93 of M-50-0.5% to 0.74 of M-50-2.25% and 0.62 of M-50-4.5%.

The permeability of M − 50 before healing (Fig. 15) increases exponentially with the pre-loading tensile strain. The permeability coefficient increases from 5.5×10^{-9} m/s at pre-loading strain of 0.5%–2.7×10^{-7} m/s at 4.5%, which coincides with the values of PVA-ECC with similar crack width [38,40].

4.5.2. *Resonant frequency and permeability recovery*

The crack healing of pre-cracked specimens is shown in Fig. 16. The white residue in the crack or on the crack surface is calcium carbonate crystals [29].

Resonant frequencies of pre-cracked LWHS-ECC specimens before and after each wet-dry cycle were monitored. At least three specimens were used to obtain the recovery RF. The results are summarized in Fig. 17. A higher pre-damage level leads to a lower RF of LWHS-ECC

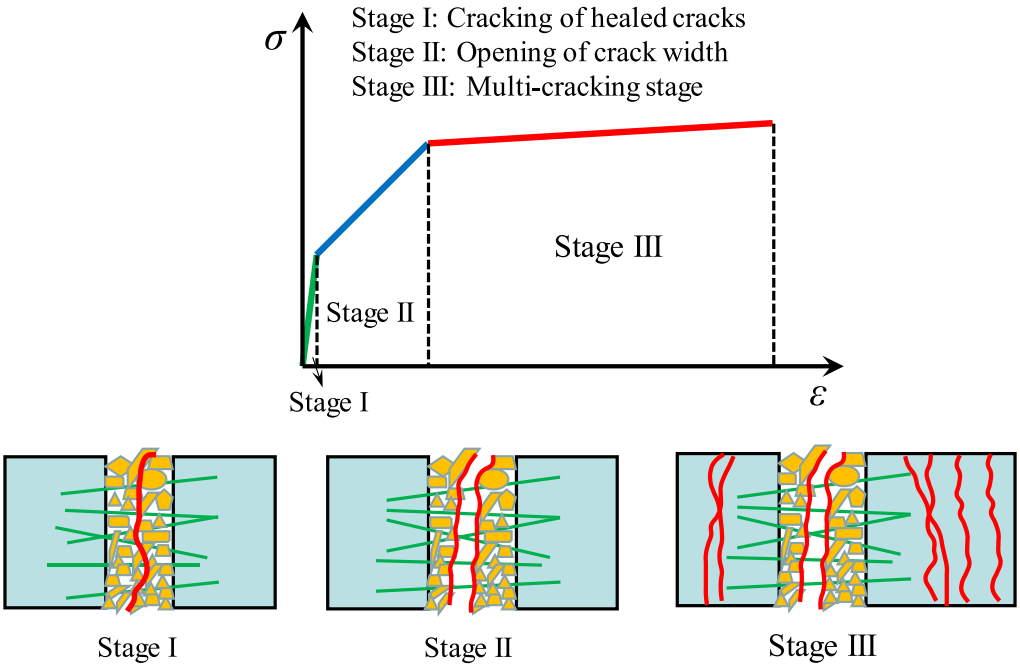

Fig. 19. Stages of re-loading tensile stress-strain curves.

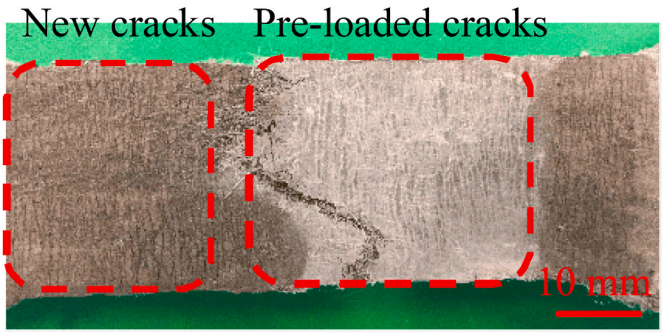

Fig. 20. Crack pattern of the re-loaded specimen of M-50-2.25%.

specimen both before and after healing due to the larger crack widths and higher crack numbers (Fig. 17a). M-50-0.5% exhibits a reduction in RF of 7.0%, while M-50-4.5% shows a reduction of 37.5%. The recovery of specimens occurs with increasing wet-dry cycles, while the RF recovers more significantly in the first 2–3 wet-dry cycles and stabilizes thereafter. The RFs of healed M-50-0.5%, M-50-2.25% and M-50-4.5% recover to 98%, 86% and 76% of the virgin specimen, respectively. The hydration products during the wet-dry cycle accumulate at the crack surface, preventing the growth of hydration products inside the micro-crack, which hinders the further RF recovery of those highly strained specimens (e.g., M-50-2.25% and M-50-4.5%). Nonetheless, the permeability of pre-cracked specimens will still benefit from the surface healing of the cracked specimens. The permeability coefficients of healed M-50-0.5%, M-50-2.25% and M-50-4.5% decrease by 97%, 92% and 86% of the pre-loaded specimen before healing, respectively (Fig. 15).

The relation between the extent of self-healing and pre-loading strain level of the LWHS-ECC specimens after the wet-dry cycle is shown in Fig. 17b. The RF recovery ratio increases with increasing pre-loading strain levels. However, the ultimate self-healing status of M-50-4.5% is notably lower than those of the specimens with lower pre-loading deformations (M-50-0.5%, 1.0%) due to its larger crack width and higher crack numbers, which limits the extent of crack self-healing (Fig. 16b).

4.5.3. *Mechanical performance recovery*

The reloading tensile stress-strain curves of healed LWHS-ECC specimens are shown in Fig. 18. All specimens with different pre-loading strains (0.5%, 1.0%, 2.25% and 4.5%) exhibit robust strain-hardening performance (Fig. 18a–c). It should be pointed out that the residual strain induced during the pre-loading stage is not accounted for in these reloading stress-strain curves. The residual crack width is approximately half of crack width at the loading state, which leads to a notable strain capacity uncounted for in highly strained specimens of M-50-4.5% (Fig. 18c and d). The tensile strength of re-loaded specimens increases with the pre-loading strain levels (Fig. 18d). The water penetrates through cracks into the LWHS-ECC matrix to enhance the interfacial bond stress and thus the tensile strength of LWHS-ECC (Fig. 18e). The more pre-cracks or higher pre-cracking strain level, the higher the ultimate tensile strength of healed LWHS-ECC.

The re-loading tensile stress-strain curves can be divided into three stages (Fig. 19). Stage I corresponds to the re-cracking of healed cracks filled with re-hydration products; Stage II corresponds to the opening of these cracks, and Stage III represents the addition of new multiple cracks. The stiffness of the re-loading specimens decreases from Stage I to Stage III due to the reopening of pre-cracks in Stage II and newly formed micro-cracks in Stage III. Further, the stiffness of LWHS-ECC specimens at Stage II decreases with increasing strain levels (Fig. 18d) due to a higher number of crack reopening, while the stiffness of LWHS-ECC specimens at Stage III increases with strain levels (Fig. 18d) due to a higher enhancement of fiber-matrix interfacial bond stress in highly strained specimens.

The crack pattern of the re-loaded specimen is shown in Fig. 20. The pre-loaded cracks are filled with white residue after healing. Newly-formed micro-cracks occur in the other areas of the gauge length during Stage III.

The tensile parameters of re-loaded LWHS-ECC specimens are summarized in Fig. 21. Both the ultimate and initial cracking tensile stresses increase with higher pre-cracking strain levels due to increased re-hydration of the LWHS-ECC matrix, which enhances the matrix fracture toughness and interfacial bond stress between fiber and matrix. The ultimate strength increases from 7.34 MPa of virgin specimens to 8.67 MPa of M-50-2.25% and 10.12 MPa of M-50-4.5%, an increase of 38% (Fig. 21a). The initial cracking stress increases from 4.18 MPa of the

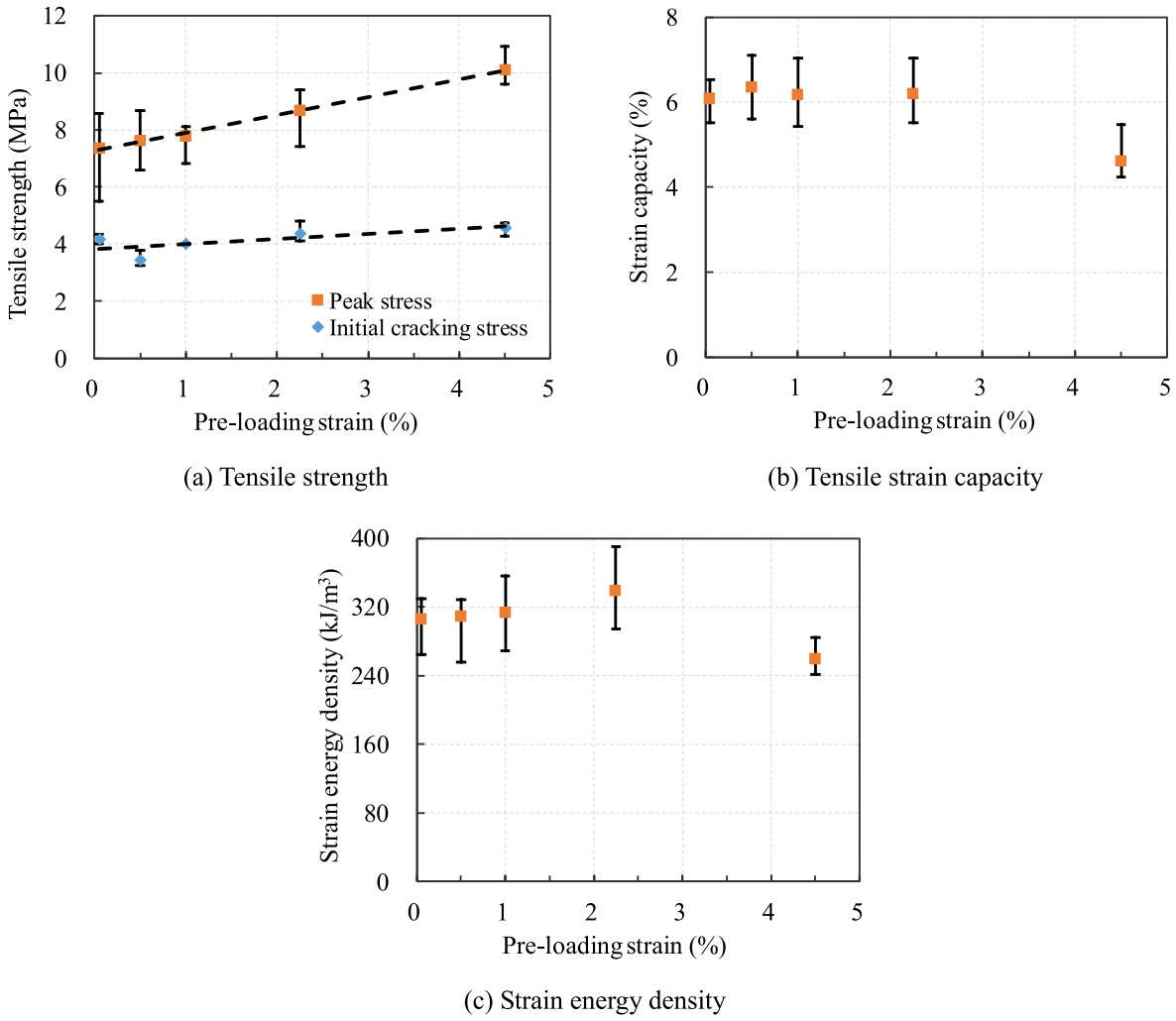

Fig. 21. Tensile parameters of reloaded specimens after self-healing.

virgin specimen to 4.59 MPa of M-50-4.5%, with an increase of 10% (Fig. 21a). The tensile strain capacity of re-loaded specimens remains at 6% up to M-50-2.25% and decreases slightly to 4.6% of M-50-4.5% due to the significant residual strain of M-50-4.5% after unloading (Fig. 21b). The strain energy density shares a similar trend with strain capacity, which increases slightly from 305 kJ/m^3 of the virgin specimen to 338 kJ/m^3 of M-50-2.25% (an increase of 11%) and decreases to 259 kJ/m^3 of M-50-4.5% (a decrease of 15%, Fig. 21c).

The tensile performances of healed LWHS-ECC vary with the pre-loading strains. Remarkably, the tensile strengths (ultimate and initial cracking strength) increase steadily with increasing pre-loading strains and are higher than those of virgin specimens. The LWHS-ECC demonstrates vigorous self-healing ability even up to 2.25% or 4.5%.

5. Conclusions

Lightweight high-strength engineered cementitious composite (LWHS-ECC) combining high tensile strength, lightweightedness and self-healing is attractive for resilient and durable infrastructures. The lightweightedness and self-healing characteristics of LWHS-ECC are realized by synergistic utilization of crumb rubber (CR) and hollow fly ash cenosphere (FAC) particles. Physical and mechanical performances of LWHS-ECC were assessed. The self-healing ability of pre-cracked LWHS-ECC under wet-dry cycles was evaluated. The detailed conclusions are drawn as follows.

1. FAC particles act as the lightweight fillers to reduce the density and the fracture toughness of LWHS-ECC matrix. CR particles act as both artificial flaws and lightweight particles to reduce matrix fracture toughness, activate more microcracks and limit crack width to ensure the self-healing potential of LWHS-ECC. The density and compressive strength of LWHS-ECC decrease with increasing amount of lightweight particles.
2. All LWHS-ECC specimens exhibit robust strain-hardening performance. The mechanical parameters, including the tensile strength, strain capacity, specific tensile strength and strain energy density decrease with the increasing proportion of lightweight particles. The specific tensile strength of LWHS-ECC is higher than that of M45 PVA-ECC. The decrease in strain capacity is caused by the reduction in crack width. Particularly, the crack width of M − 50 at ultimate tensile strength is around 50 μm, comparable to the value of PVA-ECC and endows M − 50 the self-healing potential.
3. The LWHS-ECC specimens demonstrate vigorous self-healing ability in mechanical and water transport properties. All healed specimens demonstrate stable strain-hardening behavior with newly-formed cracks. The tensile strengths of healed LWHS-ECC specimens are higher than those of virgin specimens. The wet-dry cycles notably recover the RF and permeability of LWHS-ECC specimens due to the accumulation of hydration products in the crack.

The self-healing performance of LWHS-ECC was conducted in the unloaded state in this study. Further investigation on the self-healing

performance under the loaded state is warranted in future research. In addition, the current self-healing investigation of LWHS-ECC is conducted with external water supply. The self-healing performance of LWHS-ECC specimens under low humidity environments with internal water source from super absorbent polymers remains to be investigated [41].

Declaration of competing interest

The authors declare that they have no known competing financial interests or personal relationships that could have appeared to influence the work reported in this paper.

Acknowledgements

This research has been partially supported by the University of Michigan MCubed 3 program, the UM Center for Low Carbon Built Environment, and the James R. Rice Distinguished University Professorship.

References

[1] V.C. Li, Engineered Cementitious Composites (ECC): Bendable Concrete for Sustainable and Resilient Infrastructure, Springer, 2019.
[2] Y. Yang, M.D. Lepech, E.H. Yang, V.C. Li, Autogenous healing of engineered cementitious composites under wet–dry cycles, Cement Concr. Res. 39 (5) (2009) 382–390.
[3] L.L. Kan, H.S. Shi, Investigation of self-healing behavior of engineered cementitious composites (ECC) materials, Construct. Build. Mater. 29 (2012) 348–356.
[4] Z. Zhang, S. Qian, H. Ma, Investigating mechanical properties and self-healing behavior of micro-cracked ECC with different volume of fly ash, Construct. Build. Mater. 52 (2014) 17–23.
[5] H. Liu, Q. Zhang, C. Gu, H. Su, V. Li, Self-healing of microcracks in Engineered Cementitious Composites under sulfate and chloride environment, Construct. Build. Mater. 153 (2017) 948–956.
[6] Z. Zhang, Q. Zhang, Self-healing ability of engineered cementitious composites (ECC) under different exposure environments, Construct. Build. Mater. 156 (2017) 142–151.
[7] V.C. Li, On engineered cementitious composites (ECC), J. Adv. Concr. Technol. 1 (3) (2003) 215–230.
[8] R. Ranade, V.C. Li, M.D. Stults, W.F. Heard, T.S. Rushing, Composite properties of high-strength, high-ductility concrete, ACI Mater. J. 110 (4) (2013) 413–422.
[9] I. Curosu, M. Liebscher, V. Mechtcherine, C. Bellmann, S. Michel, Tensile behavior of high-strength strain-hardening cement-based composites (HS-SHCC) made with high-performance polyethylene, aramid and PBO fibers, Cement Concr. Res. 98 (2017) 71–81.
[10] S. He, J. Qiu, J. Li, E.H. Yang, Strain hardening ultra-high performance concrete (SHUHPC) incorporating CNF-coated polyethylene fibers, Cement Concr. Res. 98 (2017) 50–60.
[11] D.Y. Lei, L.P. Guo, B. Chen, I. Curosu, V. Mechtcherine, The connection between microscopic and macroscopic properties of ultra-high strength and ultra-high ductility cementitious composites (UHS-UHDCC), Compos. B Eng. 164 (2019) 144–157.
[12] K.Q. Yu, J.T. Yu, J.G. Dai, Z.D. Lu, S.P. Shah, Development of ultra-high performance engineered cementitious composites using polyethylene (PE) fibers, Construct. Build. Mater. 158 (2018) 217–227.
[13] Y. Chen, J. Yu, C.K. Leung, Use of high strength strain-hardening cementitious composites for flexural repair of concrete structures with significant steel corrosion, Construct. Build. Mater. 167 (2018) 325–337.
[14] H. Zhu, K.T. Wan, E. Satekenova, D. Zhang, C.K. Leung, J. Kim, Development of lightweight strain hardening cementitious composite for structural retrofit and energy efficiency improvement of unreinforced masonry housings, Construct. Build. Mater. 167 (2018) 791–812.
[15] L. Li, Z. Cai, K. Yu, Y.X. Zhang, Y. Ding, Performance-based design of all-grade strain hardening cementitious composites with compressive strengths from 40 MPa to 120 MPa, Cement Concr. Compos. 97 (2019) 202–217.
[16] Y. Zhou, B. Xi, L. Sui, S. Zheng, F. Xing, L. Li, Development of high strain-hardening lightweight engineered cementitious composites: design and performance, Cement Concr. Compos. 104 (2019) 103370.
[17] Z. Zhang, A. Yuvaraj, J. Di, S. Qian, Matrix design of light weight, high strength, high ductility ECC, Construct. Build. Mater. 210 (2019) 188–197.
[18] ACI Committee 231, Guide for Structural Lightweight Aggregate Concrete, 2014.
[19] K. Wille, D.J. Kim, A.E. Naaman, Strain-hardening UHP-FRC with low fiber contents, Mater. Struct. 44 (3) (2011) 583–598.
[20] D.Y. Yoo, S. Kim, J.J. Kim, B. Chun, An experimental study on pullout and tensile behavior of ultra-high-performance concrete reinforced with various steel fibers, Construct. Build. Mater. 206 (2019) 46–61.
[21] B. Chun, D.Y. Yoo, Hybrid effect of macro and micro steel fibers on the pullout and tensile behaviors of ultra-high-performance concrete, Compos. B Eng. 162 (2019) 344–360.
[22] X. Huang, R. Ranade, Q. Zhang, W. Ni, V.C. Li, Mechanical and thermal properties of green lightweight engineered cementitious composites, Construct. Build. Mater. 48 (2013) 954–960.
[23] E.H. Yang, Y. Yang, V.C. Li, Use of high volumes of fly ash to improve ECC mechanical properties and material greenness, ACI Mater. J. 104 (6) (2007) 620.
[24] Q. Jin, V.C. Li, Development of lightweight engineered cementitious composite for durability enhancement of tall concrete wind towers, Cement Concr. Compos. 96 (2019) 87–94.
[25] D.B. Marshall, B.N. Cox, A J-integral method for calculating steady-state matrix cracking stresses in composites, Mech. Mater. 7 (2) (1988) 127–133.
[26] V.C. Li, C.K. Leung, Steady-state and multiple cracking of short random fiber composites, J. Eng. Mech. 118 (11) (1992) 2246–2264.
[27] J. Yu, J. Yao, X. Lin, H. Li, J.Y. Lam, C.K. Leung, K. Shih, Tensile performance of sustainable Strain-Hardening Cementitious Composites with hybrid PVA and recycled PET fibers, Cement Concr. Res. 107 (2018) 110–123.
[28] T. Kanda, V.C. Li, Multiple cracking sequence and saturation in fiber reinforced cementitious composites, Concrete Research and Technology 9 (2) (1998) 19–33.
[29] Y. Yang, M.D. Lepech, E.H. Yang, V.C. Li, Autogenous healing of engineered cementitious composites under wet–dry cycles, Cement Concr. Res. 39 (5) (2009) 382–390.
[30] S. Wang, V.C. Li, High-early-strength engineered cementitious composites, ACI Mater. J. 103 (2) (2006) 97.
[31] V.C. Li, S. Wang, Microstructure variability and macroscopic composite properties of high performance fiber reinforced cementitious composites, Probabilist. Eng. Mech. 21 (3) (2006) 201–206.
[32] X. Huang, R. Ranade, W. Ni, V.C. Li, On the use of recycled tire rubber to develop low E-modulus ECC for durable concrete repairs, Construct. Build. Mater. 46 (2013) 134–141.
[33] Z. Lin, V.C. Li, Crack bridging in fiber reinforced cementitious composites with slip-hardening interfaces, J. Mech. Phys. Solid. 45 (5) (1997) 763–787.
[34] A.E. Naaman, H. Najm, Bond-slip mechanisms of steel fibers in concrete, ACI Mater. J. 88 (2) (1991) 135–145.
[35] JSCE, Recommendations for Design and Construction of High-Performance Fiber Reinforced Cement Composites with Multiple Fine Cracks, Japan Society of Civil Engineers, Tokyo, Japan, 2008, pp. 1–16.
[36] F.M.C.-50 Rilem, Determination of the fracture energy of mortar and concrete by means of three-point bend tests on notched beams, Mater. Struct. 18 (106) (1985) 285–290.
[37] ASTM C215-19, Standard Test Method for Fundamental Transverse, Longitudinal, and Torsional Resonant Frequencies of Concrete Specimens, ASTM International, West Conshohocken, PA, 2019.
[38] H. Liu, Q. Zhang, C. Gu, H. Su, V.C. Li, Influence of microcrack self-healing behavior on the permeability of Engineered Cementitious Composites, Cement Concr. Compos. 82 (2017) 14–22.
[39] K. Yu, Y. Ding, J. Liu, Y. Bai, Energy dissipation characteristics of all-grade polyethylene fiber-reinforced engineered cementitious composites (PE-ECC), Cement Concr. Compos. 106 (2020) 103459.
[40] H.L. Wu, Y.J. Du, J. Yu, Y.L. Yang, V.C. Li, Hydraulic conductivity and self-healing performance of engineered cementitious composites exposed to acid mine drainage, Sci. Total Environ. 716 (2020) 137095.
[41] D. Snoeck, N.D. Belie, Autogenous healing in strain-hardening cementitious materials with and without super absorbent polymers: an 8-year study, Frontiers in Materials 6 (2019) 1–12.